AERODYNAMIC DESIGN OF THE STANDARD CLASS SAILPLANE ASW-24

by L.M.M. Boermans

Delft University of Technology, Faculty of Aerospace Engineering, The Netherlands

and G. Waibel

Alexander Schleicher, Segelflugzeugbau, West Germany

Presented at the XX OSTIV Congress, Benalla, Australia (1987)

1. Introduction

The ASW-24 is a new high performance glider for the FAI Standard Class, built by Alexander Schleicher Segelflugzeugbau, Germany. It is the successor of the ASW-19, which was built by Schleicher for more than 10 years. With the exception of some fittings, the ASW-24 is a complete new design of all components. This applies to the aerodynamic shape as well as to the materials used. Wing, fuselage and tailplane are all constructed of carbon, aramid and glassfibers. This paper is focused on the aerodynamic design of the ASW-24 which took place in close cooperation between Alexander Schleicher Segelflugzeugbau and the Delft University of Technology (DUT) Low Speed Laboratory (LSL).

A three-view drawing and some technical data are presented in Figure 1 and Table 1.

2. General design considerations

Though a high priority was given to the flight performance, great value was also set on good flight characteristics, active as well as passive safety measures and easy maintenance. It is undisputed that such balance produces the utmost efficiency of the team pilot plus glider.

Adequate horizontal and vertical tail area, elevator and rudder area and aileron area are provided for good stability and control. Examples of active safety devices are the automatic connections of all controls at their assembly points. The rubber suspended landing gear with big 5.00-5 wheel and hydraulic disk brake, and the double-panelled airbrakes. Passive safety is provided by progressive strength of the cockpit, a new design of the cockpit sidewalls which provide the view of a big canopy, together with a small cutout of the

Table 1: Technical data and estimated characteristics of the Standard Class Sailplane ASW-24

Airworthiness substantiation in accordance with JAR-22, Category U, and with the preliminary LBA-Substantiation-Requirements for gliders out of fiber compound materials.

Model		ASW 24	
Use		Training and performance flights, competition flights in the FAI Standard Class, cloud flying, and semi-aerobatics.	
Span		15,00 m	
Wing area		10,00 m²	
Aspect ratio		22,5	
Fuselage length		6,55 m	
Cockpit seating height		0,80 m	
Cockpit width		0,64 m	
Height at fin		1,30 m	
Empty mass	ca.	220 kg	
Max. flight mass		500 kg	
Mass of one wing	ca.	57 kg	
Max. of wing loading	ca.	50 kg/m²	
Min. wing loading	ca.	30 kg/m²	
Waterballast	max.	170 l	
Cockpit useful load	max.	115 kg	
Best L/D		43 at 105 km/h	
Min. sink		0,58 m/s	For m/S=
Min. speed		70 km/h	31,5 kg/m²
Max. speed	ca.	270 km/h	
Maneuvering speed	max.	205 km/h	
Max. speed			
for strong turbulence		205 km/h	
for aero tow		205 km/h	
for winch launch		140 km/h	
for landing gear extended		205 km/h	
for airbrakes extended		270 km/h	

Design and construction subject to change without prior notice.

fuselage structure. The instrument box folds upward for easy getting in and out by the pilot.

3. Wing

Airfoil

In a previous research program, some airfoils were designed such that just be adding material to the surface, the wing of an ASW-19B could be modified and tested in flight (Ref. 1). The design of those airfoils was based on experience gained in several investigations, which will be briefly reviewed. Windtunnel experiments on an inner wing and an outer wing segment of the original wing yielded information about the quality of the airfoils achieved in serial production, as well as the quality of the LSL airfoil analysis and design computer program. The characteristics of airfoils commonly used in Standard Class sailplanes were analysed and consequences of a rough leading edge were clarified; several airfoils showed serious separation problems in the latter case. Insect impact

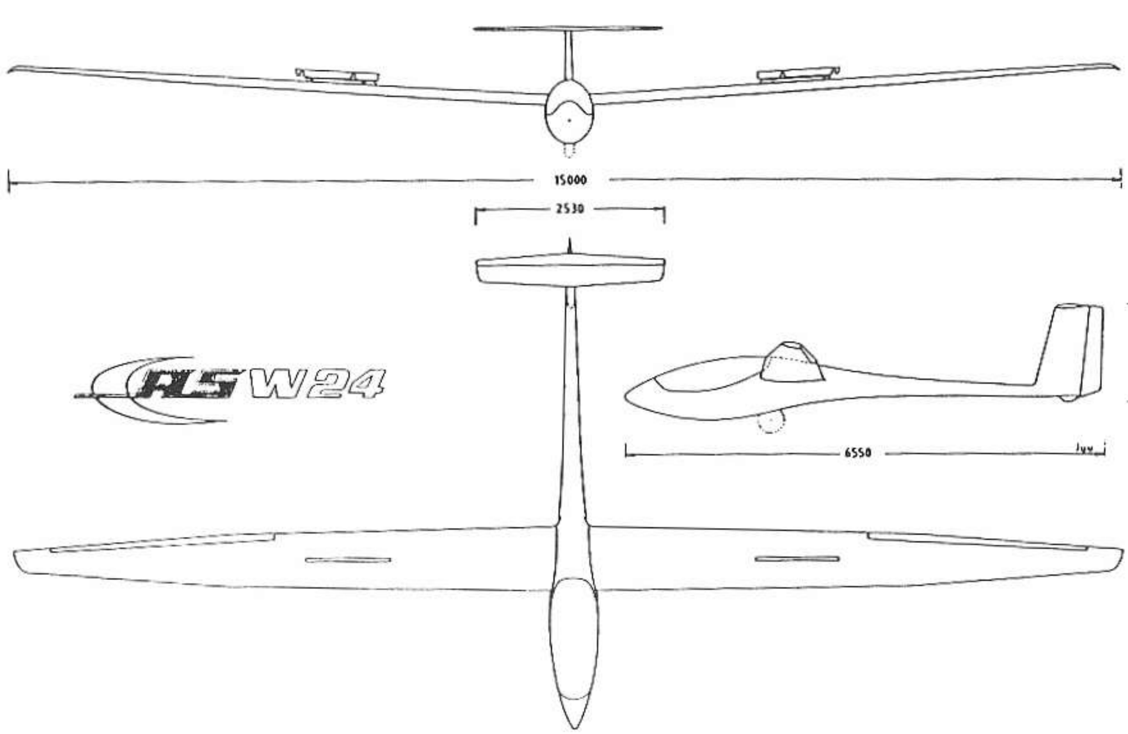

FIGURE 1. Three-view drawing of the Standard Class Sailplane ASW-24.

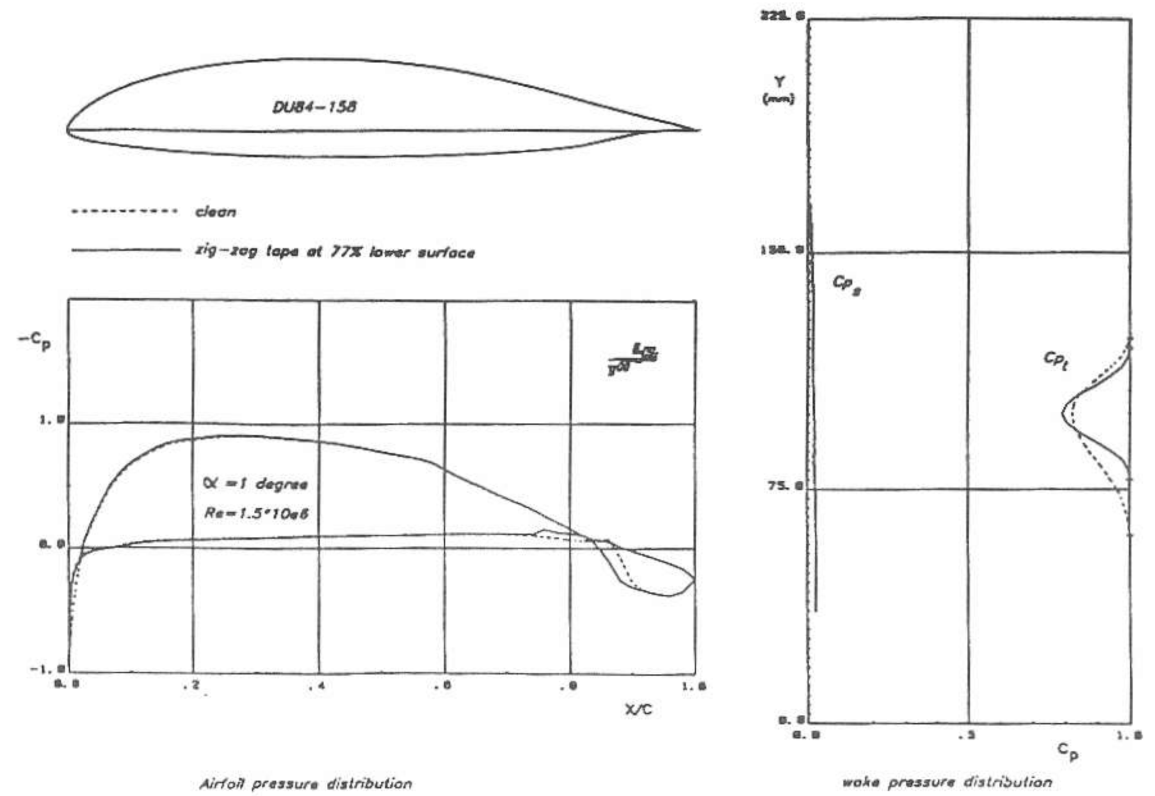

FIGURE 2. Measured airfoil and wake pressure distributions.

patterns, gathered in flight with seven different sailplanes, showed differences which are related to airfoil shape and application (e.g. flap deflection). Wind tunnel measurements on the original ASW-19B inner wing airfoil with real insect remains and with Johnson's artificial bug pattern showed the importance of the critical roughness height; insects do not always disturb the flow. Extensive wind tunnel tests showed that pneumatic turbulators — blowing air through small orifices periodically spaced in spanwise direction — can be used effectively to elminate drag producing laminar separation bubbles. Finally, sailplane performance measurements before and after the wing modification showed the success of the new airfoils: an improvement in glide ratio over the entire practical flight speed range, varying from 3 to 9%, and no change in minimum flight speed in case of a wet wing were established.

Since this research program several airfoils have been wind tunnel tested at LSL, some of them in close cooperation with DFVLR Braunschweig, and attention has been given to efficient means to provoke transition and elminate the detrimental effects of laminar separation bubbles (Ref. 2). The search for an easy-to-apply and cheap tripping device resulted in the so-called "zig-zag tape" (Ref. 3).

The airfoil designed for the ASW-24 is a further development of the airfoil deisnged for the modification of the ASW-19B inner wing, as previously mentioned. While the thickness of the latter airfoil was limited to 17.6% c as it had to fit around the existing wing, the new airfoil has a thickness of 15.8% c.

As shown in the measured pressure distributions of Figure 2, the destabalizing region concept was applied on the upper surface to avoid laminar separation bubbles. Also, the upper surface was designed for a long laminar flow region in case of a clean airfoil, while keeping the performance loss with contaminated leading edge (insects, rain) within reasonable limits. The lower surface was designed to have laminar flow up to 80% c; the detrimental laminar separation bubbles are eliminated by zig-zag tape. Measured surface and wake rake pressures indicate a laminar separation bubble on the lower surface between 80% c and 90% c, as well as only small disturbance of the smooth pressure distribution due to the zig-zag tape (positioned between 75% c and 77% c), and the corresponding wake drag reduction of 27%. Fig. 3 shows the need and effectiveness of the zig-zag tape.

In comparison to the airfoil designed for the modification of the ASW-19B inner wing, the new airfoil has lower drag at lift coefficients below $c_\ell = 1$, i.e. at interthermal penetration speeds. Considering the penetration speeds in relation to practical climb speeds and the possibility to use water ballast (up to 170 liter), the lower end of the low drag bucket was designed at $c_\ell = 0.31$ *for* $Re = 3 * 10^6$ ($c_d = .0047$).

The maximum lift coefficient is practically unaffected by roughness and the stall characteristics are seen to be soft. The moment coefficient is about 25% less than for earlier airfoils used in Standard Class sailplanes (Ref. 4). The wind tunnel model was provided with a 15% chord flap to simulate the aileron. Experiments showed that the drag produced by the slots was eliminated by flexible sealings fitted flush with the wing and sliding on the aileron upper and lower surface: the measured drag was equal to the drag of a smooth airfoil shape.

Figure 4 shows some results of tests with different position and thickness of the zig-zag tape, indicating that the tripping

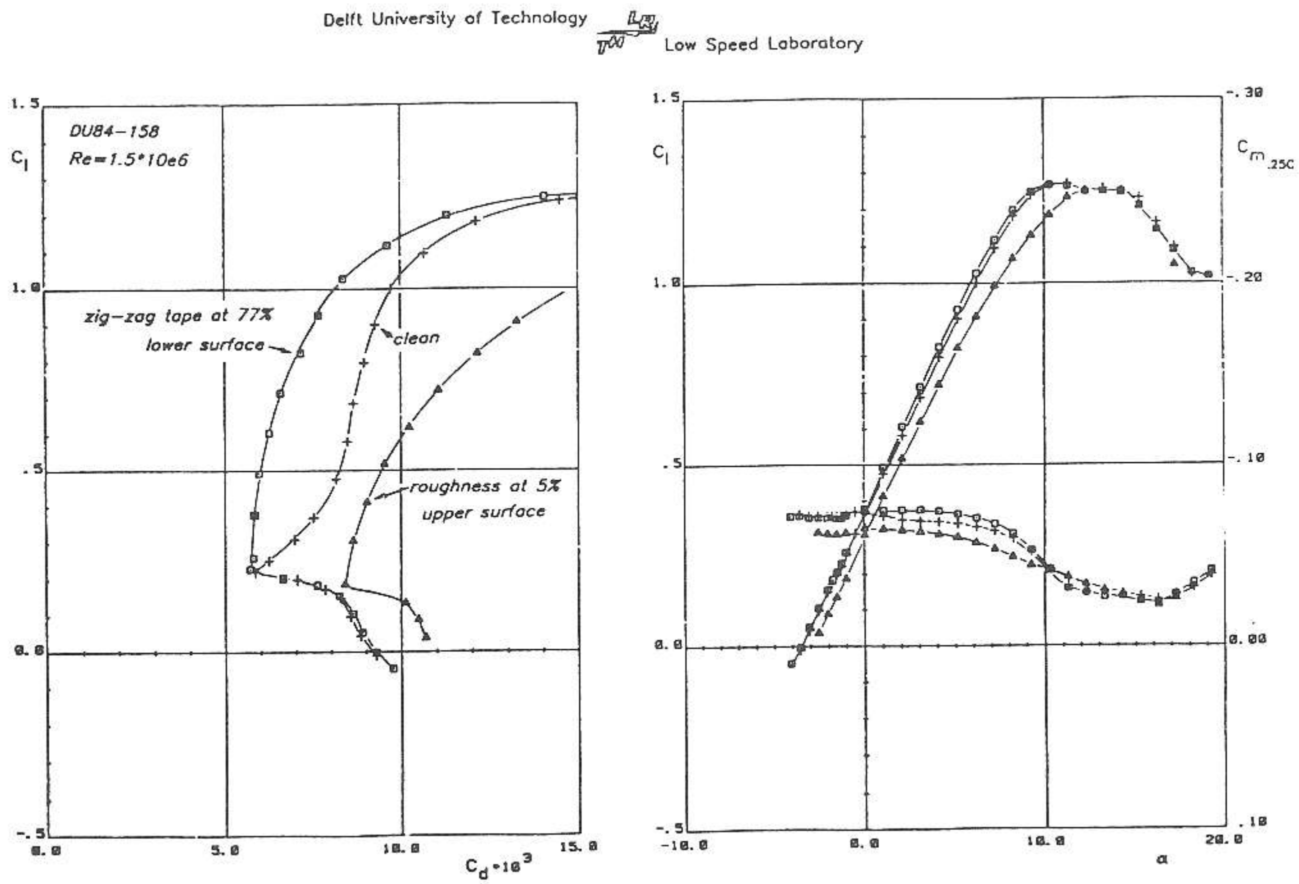

FIGURE 3. Measured aerodynamic characteristics.

device is ineffective below a certain Reynolds number, depending on thickness and psotiion of the device. Extensive tests, including flap deflections, showed that a zig-zag tape of 0.5 mm thickness, running from the wing root to the tip of the actual wing and applied at the proper chord location, may be expected to function very well at all practical flight conditions.

Recently, Dan Somers of NASA Langley Research Center drew our attention to the work of Hama (Ref. 5), where a row of thin triangular patches is proposed as being a "simple yet better way of tripping laminar boundary layers than any other known stimulation device." It is argued (Ref. 6) that this device incorporates the favorable properties of both the two-dimensional element (which produces a larger perturbation in velocity than a three-dimensional element of the same size) and the three-dimensional element (which produces vortices that will go turbulent sooner than will two-dimensional disturbances).

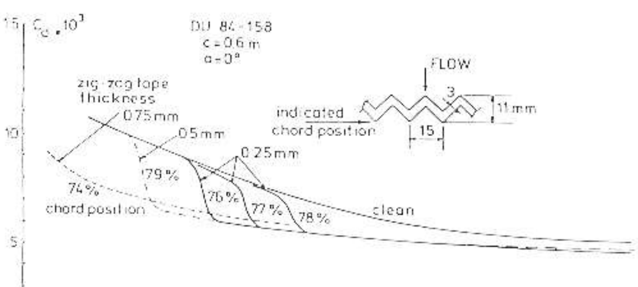

FIGURE 4. Effect of position and thickness of zig-zag tape on the drag.

According to Ref. 7 the minimum size of a trip required to result in transition at the trip without incurring undue extra drag to it, is characterized by a critical roughness Reynolds number R_k (based on the roughness height k and the velocity U_k in the undisturbed boundary layer at the height k) of about 300 for two-dimensional and 600 for three-dimensional roughness. Analysis of the measurements on DU 84-158 showed a mean critical roughness Reynolds number of zig-zag tape of 175, which indicates the effectiveness of this type of triangular tripping device.

The traces of the vortices produced by the zig-zag tape are clearly visible in fluorescent oil flow patterns, Figure 5.

Planform

To find the planform for double and triple taper wings which produce the least induced drag, Dr. J.L. de Jong of the Eindhoven University of Technology, Department of Mathematics, developed a computer program where this linearly constrained minimization problem was solved by a projected gradient type method that used the Davidson-Fletcher-Pauwel (DFP) algorithm in the linear space tangent to the intersection of the active set of constraints. The calculations are based on lifting-line theory assuming linear section lift data, the spanwise distribution of circulation is expressed in terms of Fourier series.

Figure 6 shows results for an aspect ratio of 20 and taper ratio at the tip of 0.3 and 0.4. Starting with an arbitrary plan-

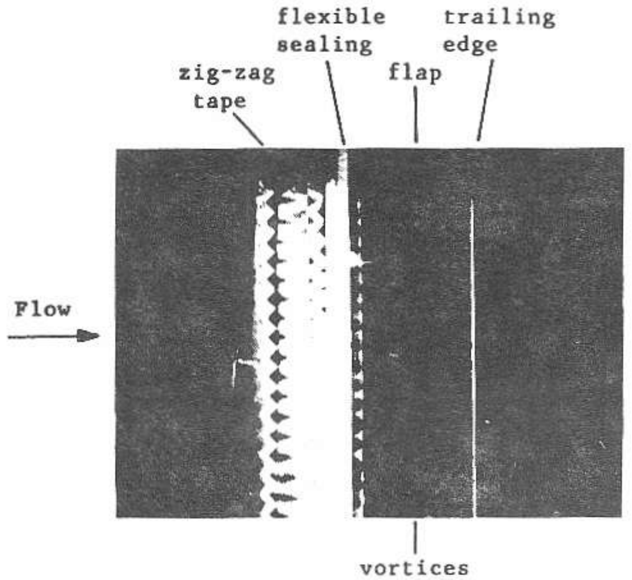

FIGURE 5. Flourescent oil flow pattern with zig-zag tape.

form (with prescribed tip taper ratio) the calculation for the double taper wing converges to a single-combination of inner wing taper and spanwise position of taper ratio change, which produces the least induced drag. In case of a tiple taper wing, however, the results showed that many planforms have an induced drag deviating less than 0.1% from the least possible value. At equal tip taper the difference in induced drag between these double and triple taper wings is negligible. For construction ease, it was decided to stick to the double taper wing.

To take profile drag into account and to estimate roll control at stall conditions, the characteristics of several wings with A = 22.5 were calculated by the method of Sivells and Neely (Ref. 8), using the measured airfoil data. Starting with the double taper wing with tip taper ratio 0.3 of Figure 6, systematic variations with respect to taper ratio and washout in the inner and outer wing were studied. The final result, being the double taper wing previously mentioned with a washout of −0.85 degrees in the outer wing, showed the least total drag at all lift coefficients in combination with adequate (expected) roll control at stall conditions; additional twist due to aerodynamic load has been taken into account.

The lift curve of the ASW-24 wing is shown in Figure 7; except for a slightly lower maxium lift coefficient, the curve is similar to that of the ASW-19B wing, which has a very gentle stall.

Aspect ratio

As previously described, the search for a thin airfoil with low drag in clean condition and acceptable performance in the contaminated case, resulted in improved performance at interthermal penetration speeds. The most effective way to improve wing performance at higher lift coefficients i.e. climbing conditions, is to increase the aspect ratio. Figure 8 shows the effect for the ASW-24 configuration with a wing aspect ratio of 20 — which is representative for Standard Class sailplanes — and with the finally chosen aspect ratio of 22.5.

The speed-polars are calculated with the computer program for parametric sailplane performance optimization described in Ref. 9. In recent years, this program has been extended

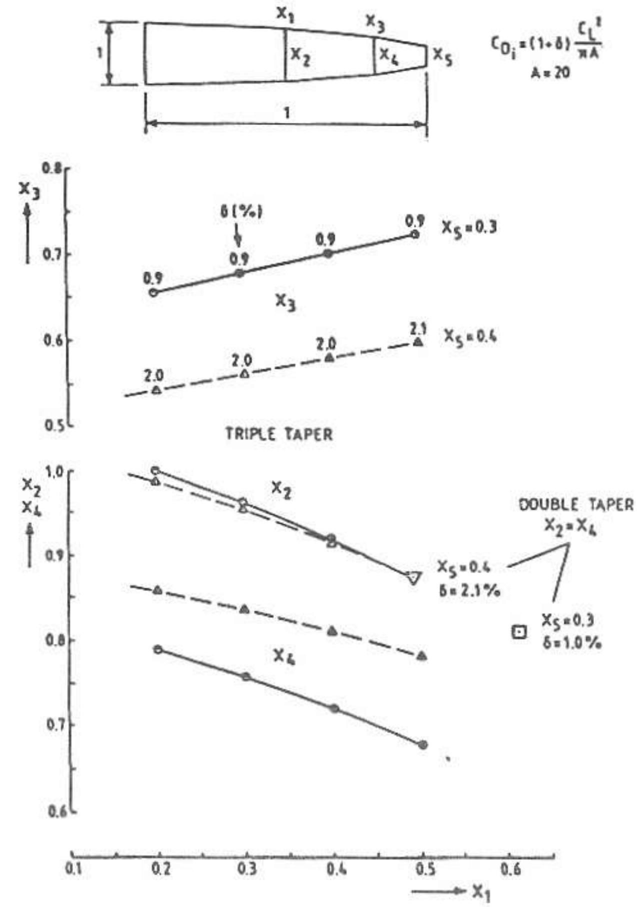

FIGURE 6. Double and triple taper wings producing least induced drag.

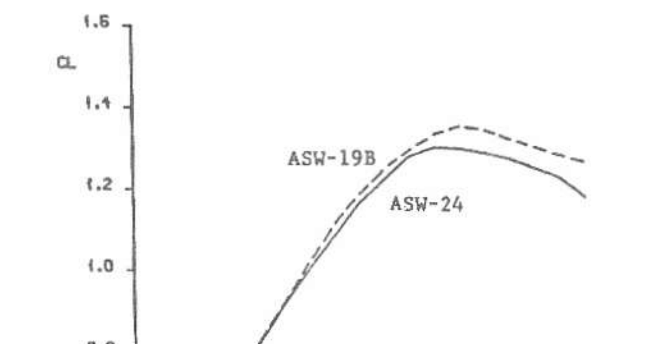

FIGURE 7. Lift curves of the ASW-19 and the ASW-24 wing.

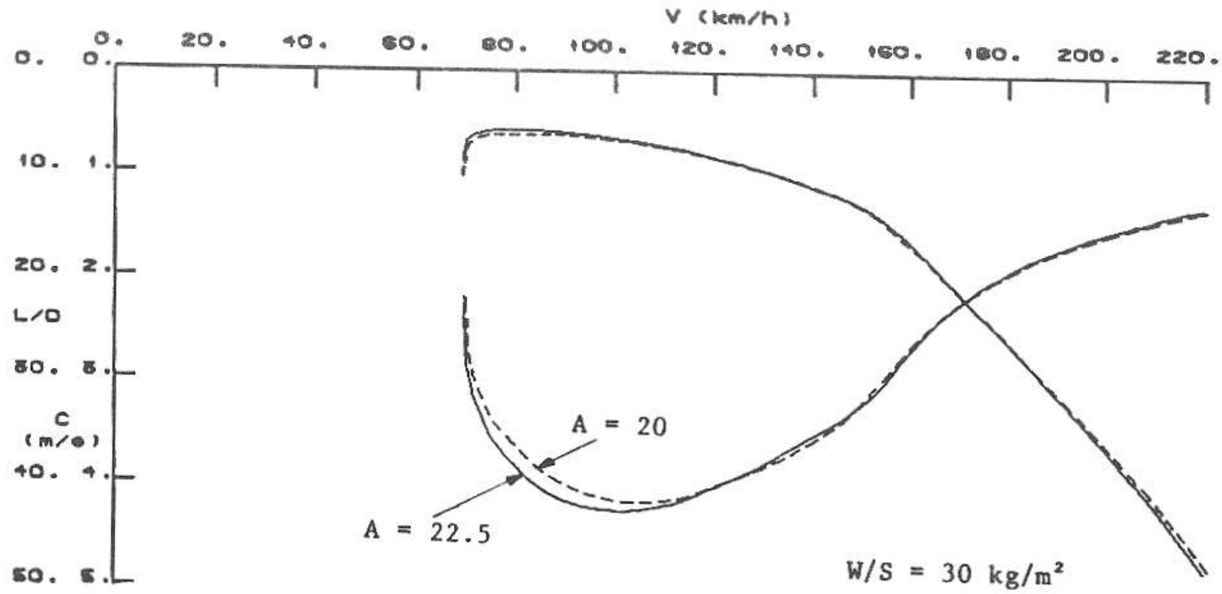

FIGURE 8. Speedpolars of the ASW-24 configuration with aspect ratio 20 and 22.5.

with the previously mentioned method of Sivells and Neely for nonlinear section lift data, and with the weather model of Kupper (Ref. 10). Moreover, the program has been implemented on the interactive CAD system of DUT, Faculty of Aerospace Engineering.

The program was used to study the effects of wing loading and aspect ratio on cross country performance in various weather conditions, Kupper composed a weather model, based on measurements of thermals (Ref. 11), flight experience and some assumptions, which is supposed to be relevant for normal central European weather conditions. Essential feature of this model is that the strength of wide and narrow thermals — in which a typical Standard Class sailplane with W/S = 32 kg/m² and A =20 climbs with 30 respectively 45 degrees angle of bank — are assumed to be distributed over the flight trajectory according to the statistical normal distribution. The climb velocity of this typical sailplane in narrow and wide thermals is the same at equal relative trajectory distance; for instance in the mean wide and narrow thermal strength which are most frequently present, i.e. over

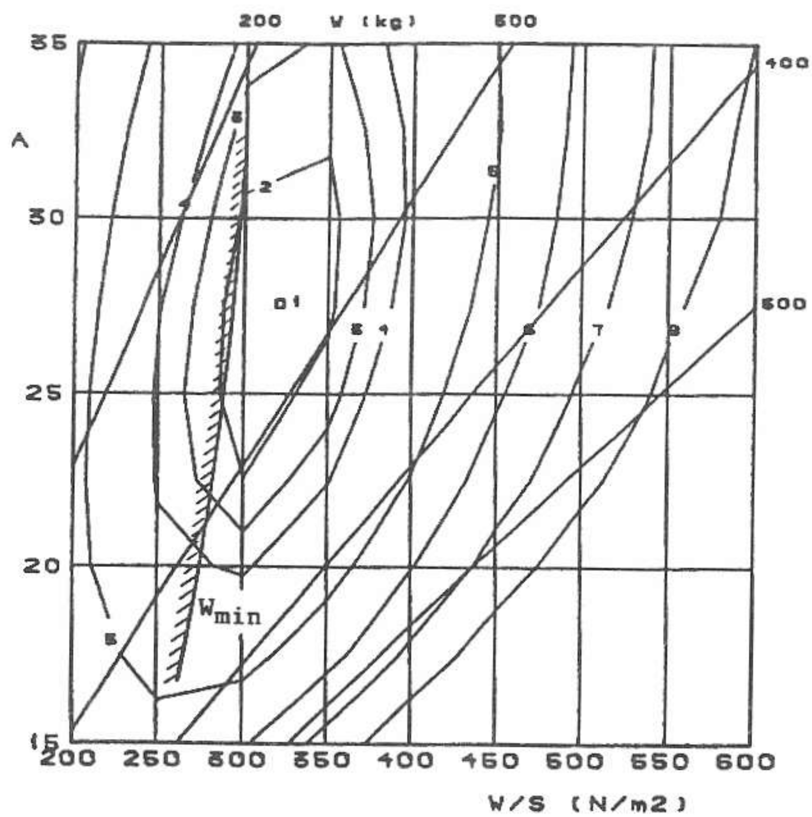

FIGURE 9. Cross-country speeds for the ASW-24 configuration in Kupper's weather model.

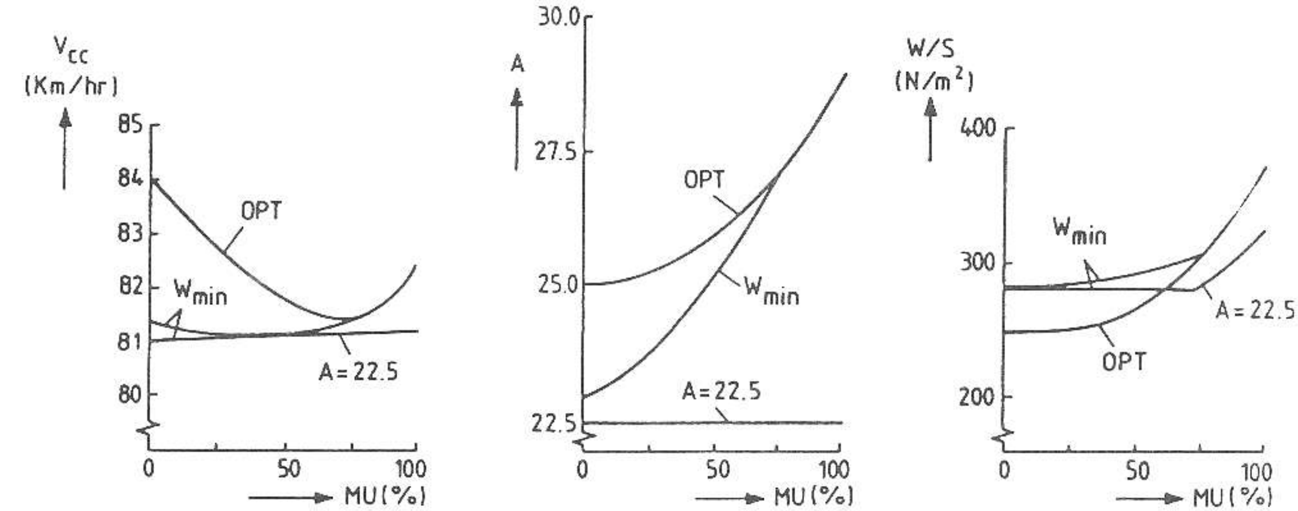

FIGURE 10. Cross-country speed, aspect ratio and wing loading for the ASW-24 configuration at various normal weather models.

the largest relative trajectory distance, this sailplane climbs with 1.6 m/s. Finally, the proportions of the trajectory with wide and narrow thermals are assumed to be 85% respectively 15%. In these weather conditions, an ASW-19B (A = 20.5) with W/S = kg/m² has a cross-country speed of 70.2 km/hr.

Figure 9 shows the results for the ASW-24 configuration where the wing loading and aspect ratio are varied; the tailplanes are adjusted to the wing aspect ratio as described in Ref. 9. As shown, the optimal aspect ratio is 27.5 at a wing loading of 32.5 kg/m², and the cross-country speed is 81.6 km/hr. With the wing loading and aspect ratio of the ASW-19B previously mentioned, the cross-country speed is only 2% lower, 80 km/hr, which indicates the flatness of the optimum.

Earlier studies, based on simpler weather models, resulted in an optimal aspect ratio between 15 and 20 (Ref. 11-15). Analysis showed that the wide thermals, which are present over a relatively large proportion of the trajectory in Kupper's model, ask for high aspect ratios. Due to the assumption of equal climb velocity in narrow and wide thermals as described before, variation of the trajectory proportions with wide and narrow thermals has no effect on the cross-country speed of the typical Standard Class sailplane, which was used to implement flight experience in the weather model. However, such alternatives of the normal weather model ask for other optimal combinations of aspect ratio and wing loading. As shown in Figure 10, a decrease of the proportion with wide thermals, denoted by MU (and increase of the proportion with narrow thermals, 1-MU) results in lower optimal aspect ratios and corresponding wing loadings. However, the wing loadings become unpractically low; in these cases the (estimated) minimum possible wing loading, Figure 9, determines the maximum attainable cross-country speed and corresponding aspect ratio. The flatness of the optimum, as previously noted, declares the good performance of a wing with aspect ratio 22.5 at corresponding optimal or minimal wing loading.

A further study with eight different weather models, composed by varying the strength of the narrow and wide thermals and their proportion of the trajectory such that the cross country speed of the typical Standard Class sailplane remains constant, resulted in optimal aspect ratios between 24 and 27.5 at wing loadings between 25 and 30 kg/m². With minimum practical wing loadings taken into account, the conclusion was the same as before. Stronger weather conditions ask for lower aspect ratios and higher wing loadings. Again, it can be shown that an aspect ratio of 22.5 combined with the proper wing loading (water ballast) give cross country speeds which differ negligibly from the optimal values.

Taking it all in all, an aspect ratio of 22.5 provides for an excellent compromise in various weather conditions.

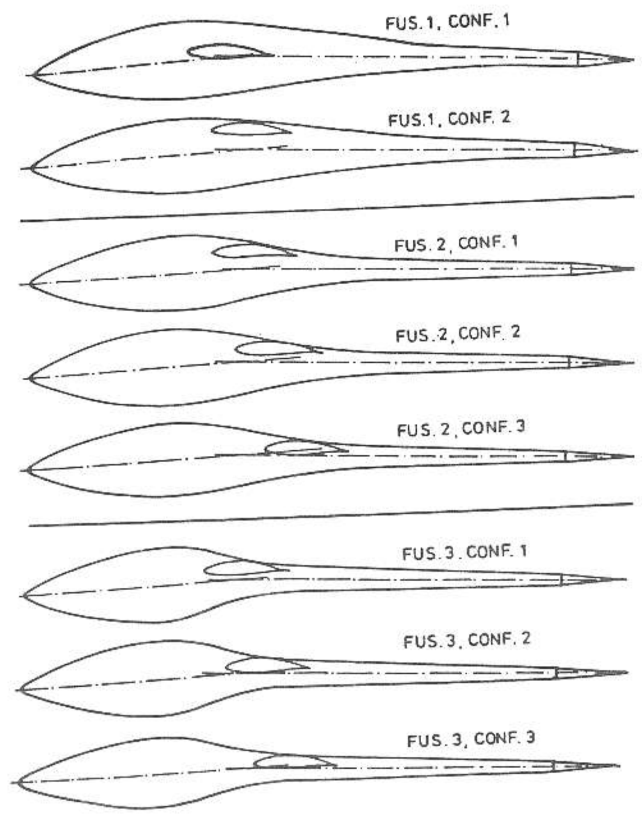

FIGURE 11. Wing-fuselage combinations tested at LSL.

4. Fuselage

In a previous research project, eight sailplane wing-fuselage combinations were wind tunnel tested at LSL, Ref. 16. The combinations were obtained by combining three different fuselages with the central section of a wing at various positions, Figure 11. The basic fuselage, no. 1, was a 1:3 scale model of the ASW-19 and ASW-20 fuselage, which was chosen because analysis of measured sailplane speed polars indicated a relatively low fuselage drag. Fuselage 2 and 3 had the same forebody as fuselage 1, but differed in contraction ratio behind the location of maximum thickness and had a 1/3 thinner tailboom. The wing segment had the Wortmann airfoil FX62-K-131/17.

Comparison of the drag results showed a significant and essentially equal drag reduction for the waisted fuselages 2 and 3 with respect to fuselage 1, primarily due to the reduction in wetted surface. Considering friction and pressure drag, the optimum contraction ratio is obviously closely met. Therefore, these contractions served as a guideline to the design of the ASW-24 fuselage contraction.

The wind tunnel results also showed the importance of streamline shaping, i.e. fitting the forebody to the streamlines of the wing to minimize crossflow effects. This crossflow effectively increases the angle of attack at the wing root area (up to approximately one fuselage diameter from the junction for a mid wing configuration), thus causing drag increase and eventually early separation at higher angles of attack. Also, at a rearward position of the wing, the accumulation of boundary layer air coming from the forebody and flowing over the upper surface of the fuselage, running up against the successive adverse pressure gradients of the fuselage, contraction and induced by the wing, leads to thick boundary layers and consequently higher drag. Therefore, the very small drag reduction measured for a rearward wing location at low lift coefficients does not outweigh the drag increase at higher lift coefficients (let alone the structural consequences of negative wing sweep for center of gravity reasons).

The forebody centerline of the ASW-24 fuselage is parallel to the streamlines of the wing at a lift coefficient of 0.85. The upper and lower forebody contour are derived from the Wortmann FX71-L-150/30 low drag airfoil, using the expression given by Galvao (Ref. 17):

$$r = y^{3/2}$$

by which a two-dimensional airfoil shape (y) can be transformed into a three-dimensional body (r), having approximately the same super-velocity at maximum thickness (and not the same velocity gradient along the contour as stated by Galvao). The resulting smooth thickness distributions are laid off perpendicular to the body centerline. A similar procedure is followed for the width at the forebody centerline. The cross sections of the fuselage are defined by a mathematical expression (Hugelschaeffer curves) having continuous curvature (for smooth velocity distributions) along the contour. The fuselage centerline behind the wing is parallel to the streamlines of the wing at a lift coefficient of 0.6, the dimensions of the tailcone are limited by structural stiffness requirements.

Overall, the wetted surface of the fuselage is about 20% less than for other modern production type Standard Class sailplanes.

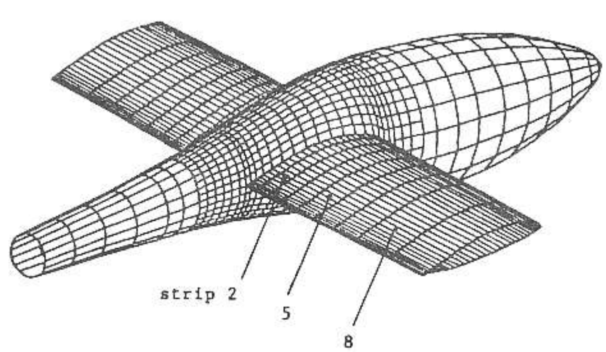

FIGURE 12. Part of panel scheme of ASW-24 wing-fuselage combination.

Wing-fuselage combination

In order to check the pressure distributions on the wing and fuselage and to study wing-fuselage interference effects, a first-order panel method developed at NLR (Ref. 18) has been applied. The surface of the wing and fuselage is represented by a large number of quadrilateral panels, each carrying a source distribution of constant strength, thus taking the thickness effects into account. A system of horse-shoe vortices on the skeleton surface and prolonged into the wake takes the lift effects into account. The shape of the wake is fixed in order to maintain the problem linear; in most practical cases, the errors so introduced are negligible. Considering that viscous effects are not taken into account, the qualitative agreement between measured and calculated pressure distributions for attached flow conditions are excellent (Ref. 18, 19).

A total number of about 3000 panels was used to model the ASW-24 wing-fuselage combination. Figure 12 shows the interesting part; the density of the panels in the junction area was increased to obtain detailed pressure distributions. The panel scheme was produced by means of the CAD system using an interactive computer program developed for this purpose; hence, it is relatively easy to model and modify the geometry.

Figure 13a shows pressure distributions along the top and bottom of the fuselage at a lift coefficient of about 1.1. The pressure gradients due to fuselage contraction and induced by the wing on the top of the fuselage are properly combined to postpone transition. The flat pressure distribution on the bottom of the fuselage, below the pilot's seat, may cause earlier transition. To assure an aft position of transition, the bottom line and cross sections were slightly modified (not shown here). Figure 13b shows the pressure distribution on the fuselage along a row of panels running just above and below the wing. The pressure rise induced by the wing upper surface deserves special attention, although oil flow studies on the eight combinations indicate no separation problems on the fuselages. On the contrary, the pressure rise induced by the wing root stagnation pressure causes the laminar forebody flow to become turbulent first, and then to separate. A separation line around the junction is observed in the oil-flow patterns, its position depends on the angle of attack. The separated surface rolls up into a system of vortices wrapped around the wing root. The experiments also indicate that separation can be expected, due to the steep pressure rise induced by the airfoil lower surface (behind 80% c).

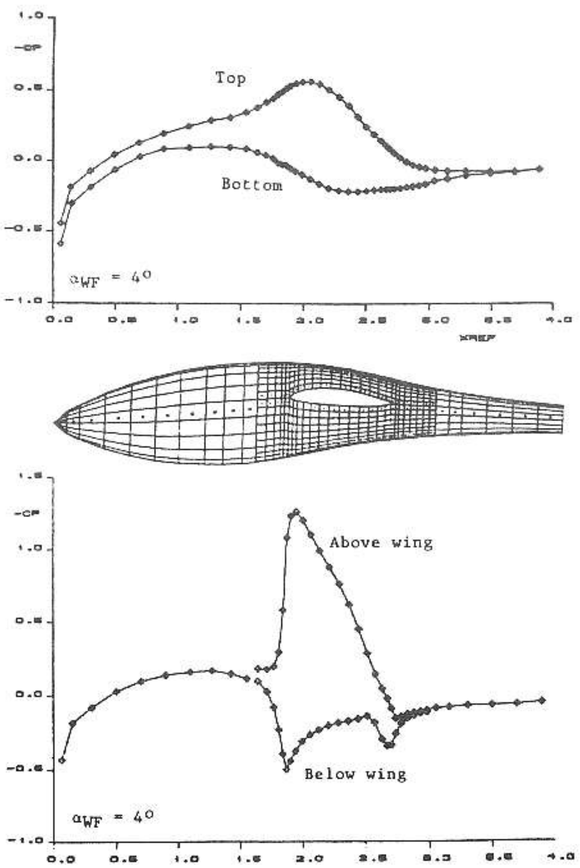

FIGURE 13a. and 13 b. Pressure distributions along the top and bottom of the fuselage and along a row of panels running just above and below the wing.

Figure 14a and 14b show pressure distributions of wing strips located within one fuselage diameter from the junction, indicating the interference effect. The consequence of fitting the fuselage forebody to the streamlines at a higher lift coefficient — thus avoiding additional suction peaks at the leading edge, Figure 14a — is an increased crossflow effect at a low lift coefficient, indicated by the lower surface pressure distributions in Figure 14b. Hence, at high speed conditions when the wing airfoils approach the lower end of the low drag bucket, a small part of the wing next to fuselage operates below the low drag bucket. This effect was also noticed in the drag measurements for all the combinations.

To improve the flow conditions at the junction, the wing is modified in the wing root area. A small fairing with 7% chord extension is applied where the wing is lofted towards a wing root airfoil designed to be suitable for turbulent flow conditions (at least in the two-dimensional case). In comparison to the wing airfoil, turbulent separation on the root airfoil upper surface is predicted to start at a higher lift coefficient, and a steep pressure rise on the lower surface has been avoided. Flight tests will have to show if this fairing is adequate. Meanwhile, research on the design of proper wing-fuselage junctions continues at LSL; the imperfections traced by the experimental and theoretical methods are, more or less, present on all existing sailplanes.

5. Tail surfaces

The horizontal and vertical tails operate at conditions (Reynolds numbers, rudder deflections) where special measures have to be taken to avoid detrimental laminar separation bubbles. Wortmann applied extensive instability regions on his well-known airfoils FX71-L-150/20, /25 and /30, designed for tailplane application (Ref. 20). The success of artificial tripping devices to avoid these bubbles, thus making longer laminar flow regions possible on sailplane wings, is the obvious reason to apply this technique also in designing new airfoils for the ASW-24 tail surfaces (Ref. 21).

The desired width of the low drag bucket for the horizontal tailplane airfoil was derived from calculating the operating range of angles of attack and elevator deflections in straight and circling flight at forward and rearward c.g. positions according to the method of Ref. 22. For safety reasons, for instance to counteract undersired motions of the airplane during cable towing or cable break, $c_{\ell_{max}}$ values were required to be comparable to the values of the Wortmann tailplane airfoils mentioned before. The desired width of the low drag bucket for the vertical tailplane airfoil was derived from slip and rudder deflection measurements with an ASW-20 in thermal flight conditions.

All modern sailplanes have a t-tail configuration in which the leading edge of the horizontal tailplane centre-line section

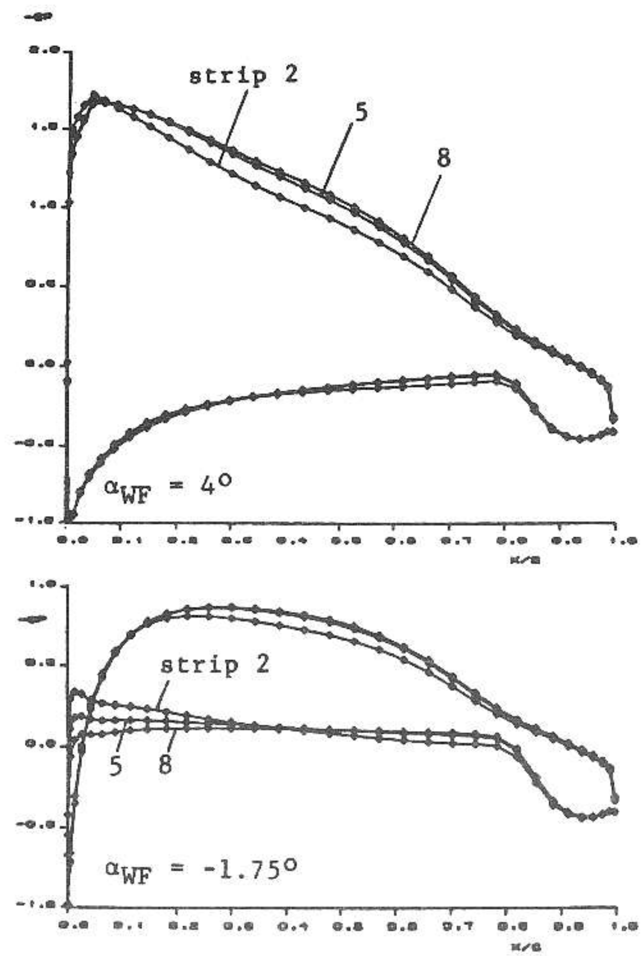

FIGURE 14a. and 14 b. Pressure distributions of wing strips in the wing root area.

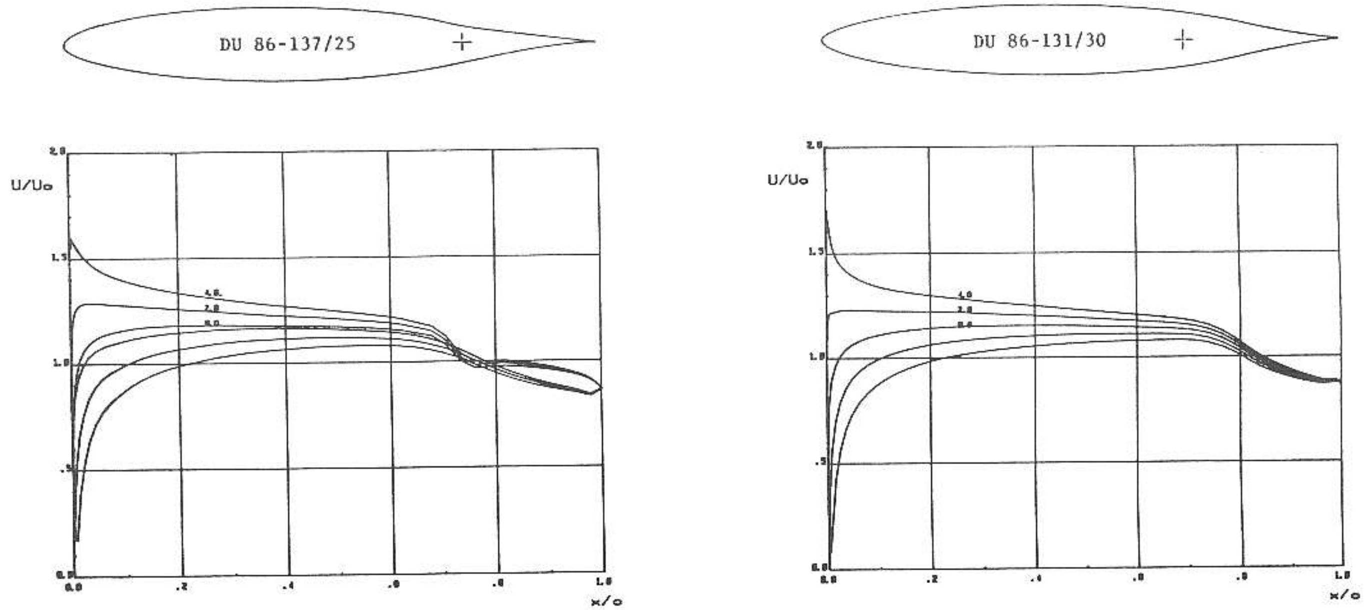

Horizontal tailplane airfoil Vertical tailplane airfoil

FIGURE 15. Horizontal and vertical tailplane airfoil and potential flow velocity distributions.

projects in front of the vertical tailplane. Similar to the wing-fuselage junction flow, the laminar boundary layer on the lower surface of the horizontal tailplane turns turbulent and separates as it approaches the vertical tailplane stagnation, and the separated flow rolls up in a system of vortices wrapped around the junction. Separated flow is observed at the rear part of the corner (Ref. 23).

To improve the flow conditions at the junction, the leading edges of the ASW-24 horizontal and vertical tailplane coincide and steep airfoil pressure gradients are avoided. The upper surface of the horizontal tailplane airfoil, however, was designed to avoid steep pressure gradients on the elevator at downward deflections (for $c_{\ell_{max}}$ reasons), hence, the horizontal tailplane is not symmetrical. Figure 15 shows the horizontal tailplane airfoil (thickness 13.7% c, elevator depth 25% c) and the vertical tailplane airfoil (thickness 13.1% c, rudder depth 30% c) and some potential flow velocity distributions. Figure 16 shows a comparison of calculated drag coefficients assuming artificial transition at the proper positions for the DU airfoils and no drag increase due to laminar separation bubbles for the FX airfoils.

The horizontal tailplane airfoil will be wind tunnel tested at LSL early 1987 for verification and to find out if the functions of zig-zag tape and flexible sealings can be integrated by cutting zig-zags in the leading edge of the sealings.

6. Concluding remarks

At the time of writing this paper, the mouldings of the

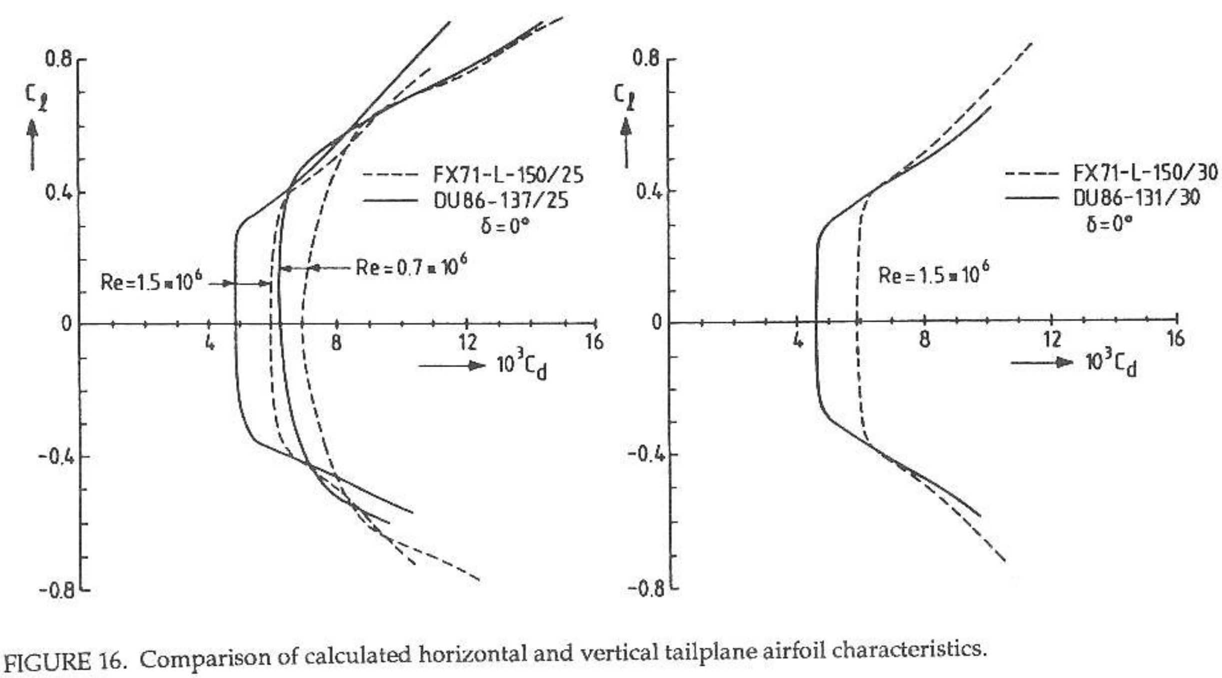

FIGURE 16. Comparison of calculated horizontal and vertical tailplane airfoil characteristics.

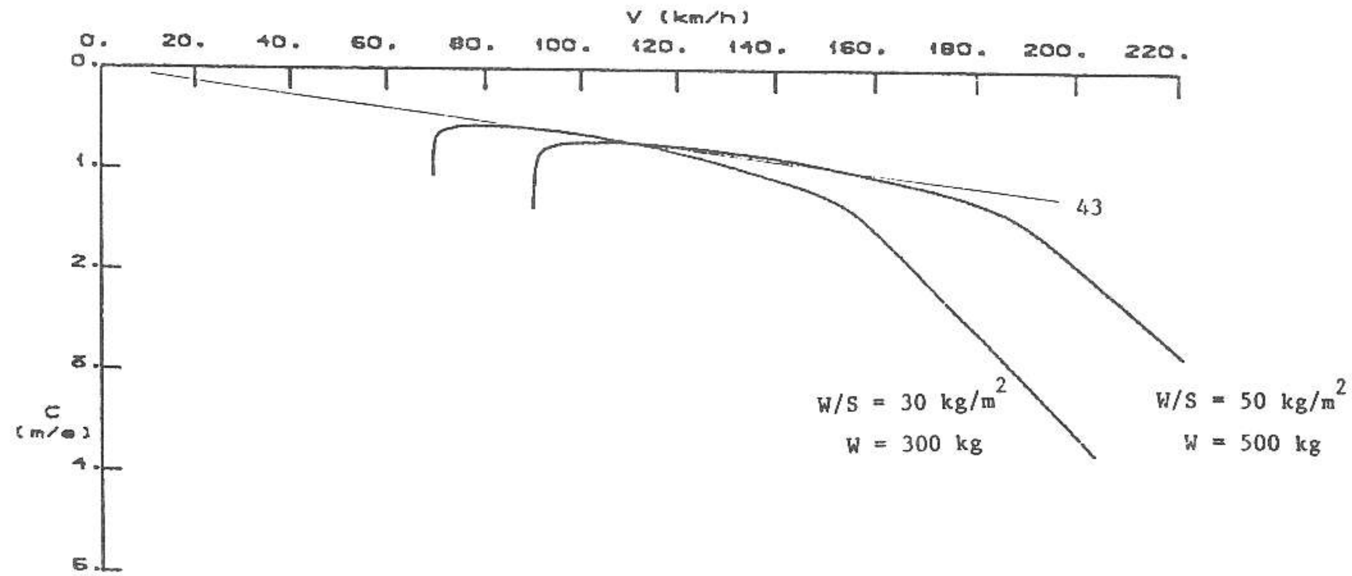

FIGURE 17. Calculated performance of the Standard Class Sailplane ASW-24.

ASW-24 master model are taken. First flight is expected in summer 1987. It has been shown that this sailplane is a new design of all components. The calculated speed polars, Figure 17, indicate that a further improvement of performance in the Standard Class may be expected.

Acknowledgments

The authors are indebted to the colleagues at the Low Speed Laboratory for their support and assistance, and to B. Oolbekkink, R.H.J. Oerlemans, L.R.J. Mulkens, J. Middel and S.J. Vermeer for their valuable contributions performed in the framework of their thesis work.

References

1. Boermans, L.M.M., Selen, H.J.W. 1982 Design and tests of airfoils for sailplanes with an application to the ASW-19B. ICAS paper 82-5.5.2.
2. Horstmann, K.H., Quast, A., Boermans, L.M.M. 1984 Pneumatic turbulators — a Device for drag reduction at Reynolds numbers below 5.10^6. AGARD CP-365, paper 20.
3. Ingen, J.L. van, Boermans, L.M.M. 1986 Aerodynamics at low Reynolds numbers: A review of theoretical and experimental research at Delft University of Technology. Proceedings of the International Conference on Aerodynamics at Low Reynolds Number, Royal Aeronautical Society, London, October 1986.
4. Althaus, D. 1972 Stuttgarter Profilkatalog I. Institut für Aero- and Gasdynamik der Universität Stuttgart.
5. Hama, F.R. 1957 An efficient tripping device. Journal of the Aeronautical Sciences, Vol. 24, no. 3, 1957.
6. Smith, A.M.O., Clutter, D.W. 1959 The smallest height of roughness capable of affecting boundary layer transition. Journal of Aerospace Sciences, April 1959.
7. Young, A.D., Paterson, J.H. 1981 Aircraft Excrescence Drag. AGARDograph 264.
8. Sivells, J.C., Neely, R.H. 1947 Method of calculating wing characteristics by lifting-line theory using nonlinear section lift data. NACA TN No. 1269.
9. Boermans, L.M.M. 1980 Development of a computer program for parametric sailplane performance optimization. OSTIV Publication XV.
10. Küpper, T. 1984 Reisegeschwindigkeit von Segelflugzeugen unter Berücksichtigung von statistischen Aufwindstärken. DFVLR-FZ Braunschweig, Unpublished student's thesis.
11. Horstmann, K.H. 1976 Neue Modellaufwindverteilungen und ihr Einfluss auf die Auslegung von Segelflugzeugen. OSTIV Publication XIV.
12. Irving, F.G. 1970 Computer analysis of the performance of 15 m sailplanes using thermals with parabolic velocity distributions. OSTIV Publication XI.

13. Irving, F.G. 1972 Computer analysis of the performance of 15 m sailplanes. NASA CR-2315.

14. Eppler, R. 1972 When should we use water ballast? NASA CR-2315

15. Boermans, L.M.M. 1978 Soaring flight optimization theory and an application in sailplane design. NVvL-Annual Report 1978.

16. Boermans, L.M.M. Terleth, D.C. 1983 Wind tunnel tests of eight sailplane wing-fuselage combinations. OSTIV Publication XVII.

17. Galvao, F.L. 1968 A note on low drag bodies. OSTIV Publication X.

18. Labrujere, Th.E. Loeve, W. Slooff, J.W. 1970 An Approximate Method for the Calculation of the Pressure Distribution on Wing Body Combinations at Subcritical Speeds. AGARD CP 71-11.

19. Baston, A. Lucchesini, M. Manfriani, L. Polito, L. Lombardi, G. 1986 Evaluation of pressure distributions on an aircraft by two different panel methods and comparison with experimental measurements. ICAS-86-1.5.3.

20. Wortmann, F.X. 1972 Symmetrical airfoils optimized for small flap deflections. OSTIV Publication XII.

21. Boermans, L.M.M. 1986 Airfoil design for the horizontal tail plane of a sailplane. Delft University of Technology Low Speed Laboratory. Internal Report LSW 86-2.

22. Stich, G. 1981 Das gedämpfte Höhenleitwerk in Kreisflug. OSTIV Publication XVI.

23. Lautanala, L. 1982 Flow visualization in the horizontal and vertical stabilizer joint area in a glider aircraft. Bericht Idaflieg Wintertagung, Heft VIII.